Ru(II) Complexes with Protic- and Anionic-Naked-NHC Ligands for Cooperative Activation of Small Molecules

Shambhu Nath,[a] Ekta Yadav,[a] Abhinav Raghuvanshi,[a] and Amrendra K. Singh*[a]

[a] Shambhu Nath, Ekta Yadav, Dr. Abhinav Raghuvanshi, Dr. Amrendra K. Singh
Department of Chemistry
Indian Institute of Technology Indore
Simrol, Indore 453552, India
E-mail: aks@iiti.ac.in
Homepage: http://people.iiti.ac.in/~aks

Supporting information for this article is given via a link at the end of the document.

Abstract: A set of ruthenium(II)-protic-N-heterocyclic carbene complexes, [Ru(NNC^{H})(PPh$_3$)$_2$(X)]Cl (**1**, X=Cl and **2**, X=H) and their deprotonated forms [Ru(NNC)(PPh$_3$)$_2$(X)] (**1'**, X=Cl and **2',** X=H) are reported where NNC is a new unsymmetrical pincer ligand. The four complexes are interconvertible by simple acid-base chemistry. The combined theoretical and spectroscopic investigations indicate charge segregation in anionic-NHC complexes (**1'** and **2'**) and can be described from a Lewis pair perspective. The chemical reactivity of deprotonated complex **1'** shows cooperative small molecule activation. Complex **1'** activates H-H bond of hydrogen, C(sp^3)-I bond of iodomethane, and C(sp)-H bond of phenylacetylene. The activation of CO_2 using anionic NHC complex **1'** at moderate temperature and ambient pressure and subsequent conversion to formate is also described. All the new compounds have been characterized using ESI-MS, ^{1}H, ^{13}C, and ^{31}P NMR spectroscopy. Molecular structures of **1**, **2**, and **2'** have also been determined with single-crystal X-ray diffraction. The cooperative small molecule activation perspective broadens the scope of potential applications of anionic-NHC complexes in small molecule activation, including the conversion of carbon dioxide to formate, a much sought after reaction in the renewable energy and sustainable development domains.

Introduction

Protic-N-heterocyclic carbene (pNHC) complexes are a class of compounds that have garnered significant attention in recent years due to their potential applications in catalysis.[1] These complexes with proton-responsive ligands have shown promising reactivity and selectivity in various catalytic reactions.[2] Anionic-naked-N-heterocyclic carbene complexes represent a relatively new and emerging class of compounds obtained from pNHC complexes after deprotonation of the N-H unit and are characterized by negatively charged NHC ligands.[3] The proton responsive nature of pNHCs and their deprotonated counterparts, anionic-NHCs, make them excellent candidates for exploring metal-ligand cooperativity (MLC)[1b,4] in complexes with NHC ligands which have, traditionally, been regarded as excellent spectator ligands.[5]

Metal-ligand cooperativity plays a pivotal role in the activation and functionalization of chemical bonds, making it an attractive strategy for efficient catalysis.[6] The cooperative interactions between metals and CH/NH/OH functionalities within the coordination sphere have been extensively documented and employed in various catalytic systems.[7] Notably, compared to the α-protic metal-amine bifunctional catalysts reported by Noyori[8] and Ikariya, complexes featuring protic N-heterocyclic carbene (pNHC) ligands exhibit a β-NH group adjacent to the metal center.[9] In β-protic pNHC complexes, these two reactive centers are electronically conjugated through π-electron systems, despite being more spatially separated. The unique characteristics of pNHC complexes enable the activation of H_2 and CO_2 at the metal center through interaction with the deprotonated NH-wingtip,[2e-f,48] while also serving as a molecular recognition unit for substrates via hydrogen bonding.[2c,3c,11]

Frustrated Lewis pairs (FLPs), since the pioneering work by Stephan and Erker, have grown into an exciting field of chemistry which parallels the cooperative action of two components traditionally observed for MLC based systems.[12] MLC, though, predates and is distinct from FLP chemistry,[13] shares a complementary strategy for activating and functionalizing small molecules.[14] Recent developments with the so called transition metal frustrated Lewis pairs (TMFLPs) incorporating transition metals into FLP chemistry have opened up new possibilities for the exploration of rich chemistry and their applications in the field of small molecule activation and catalysis.[15] Expanding the reactivity scope of MLC by leveraging principles and reactions from main-group FLPs,[14e,16] or designing novel backbones for pre-organized intramolecular main-group FLPs based on the extensive knowledge of ligand design could unlock further potential for both approaches in various applications.[17] It has further been proposed that looking at MLC systems from a Lewis pair perspective could offer fresh insights for developing a wider area of “cooperative” catalysis.[18] In this regard, the pair of complexes with pNHC and their deprotonated anionic-NHC ligands present an intriguing set of complexes which can be used to describe this “parallelism” between MLC and FLP concepts. While the pNHC complexes appear similar to the traditional MLC systems, their anionic-NHC analogues can be looked at as having Lewis pairs (Figure 1).

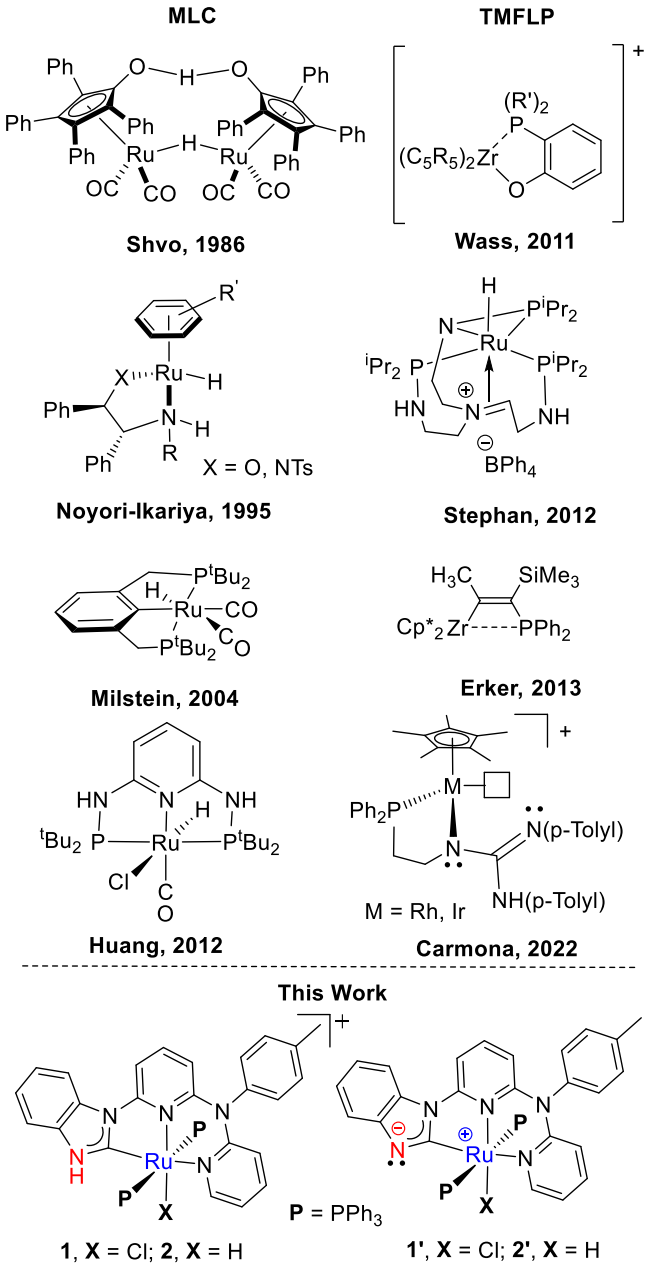

Figure 1 Representative examples of complexes showing MLC and TMFLP behaviour.

Herein, we have explored the reactivity of protic-NHC complexes **1** and **2** bearing a new unsymmetrical NNC ligand framework. The deprotonation of NH functionality of the Ru(II) pNHC complexes led to the formation of *β*-deprotonated NHC complexes **1'** and **2'**. Experimental and theoretical studies show that the *β* -deprotonated nitrogen in complexes **1'** and **2'** tends to behave as Lewis basic site while the metal itself can be considered as a Lewis acid. Complex **1'** shows metal-ligand cooperativity, which has been utilized in the activation of H_2, CO_2, phenylacetylene, and iodomethane. The reactivity pattern can be looked at as "cooperative" action of Lewis pairs to describe the metal-ligand cooperativity of these systems, as few other systems have been described by Wass and coworkers.[18d]

Results and Discussion

Synthesis and characterization

The unsymmetrical NNC pincer ligand 6-(1*H*-benzimidazol-1-yl)-N-(pyridin-2-yl)-N-(p-tolyl) pyridin-2-amine, **L1** was synthesized in three steps as shown in Scheme 1. Precursors **a** and **b** have been prepared by known literature procedures.[19] **L1** was obtained in 66% yield by the Pd-catalyzed Buchwald-Hartwig cross-coupling reaction of **a** and **b**.[20] ^{1}H, ^{13}C{^{1}H}, and 2D (^{1}H-^{1}H COSY, HSQC and HMBC) NMR spectroscopy was used to characterize ligand **L1**. In addition, the HRMS(ESI$^+$) supports the formation of **L1** with a corresponding peak for $[M+H]^+$ at m/z = 378.1722 (see SI). The reaction of **L1** with an equimolar amount of $[RuCl_2(PPh_3)_3]$ in methanol for 12 hours at 65 °C led to the formation of cyclometallated $[Ru(NNC^H)(PPh_3)_2(Cl)]Cl$ complex **1**, which was isolated as a pale-yellow powder in 56% yield. The identity of **1** was confirmed by NMR, SCXRD, Mass and IR spectroscopy.

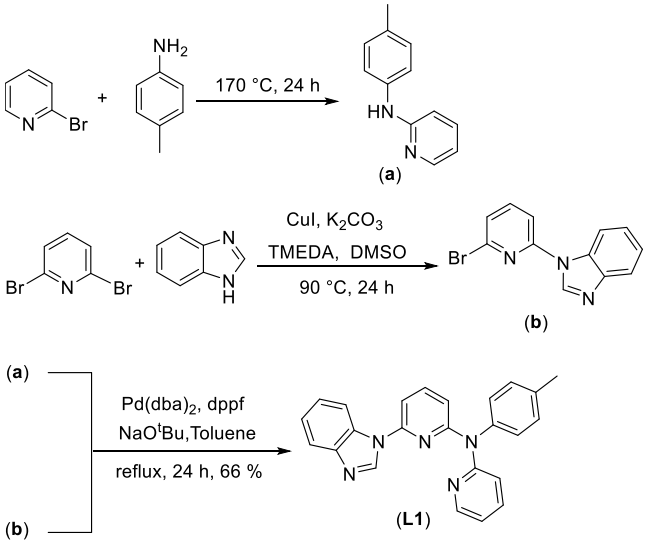

Scheme 1 Synthesis of unsymmetrical NNC pincer ligand **L1**

The multinuclear NMR studies of **1** in dmso-d_6 indicated a dynamic equilibrium between **1** and its phosphine dissociated form. ^{1}H NMR spectrum of **1** shows two peaks at *δ* 14.15 and 13.97 ppm for the NH protons.[21] In addition, the pyridyl ortho protons also display two doublets at *δ* 9.34 and 9.07 ppm, with two sets of signals for other aromatic protons. ^{31}P{^{1}H} NMR spectrum also shows two peaks at *δ* 23.89 and 32.44 ppm, along with a peak at -6.00 ppm for free triphenylphosphine ligand in solution.[1f,22] In ^{13}C{^{1}H} NMR, the resonance for Ru–$C_{carbene}$ as triplet signal observed at *δ* = 204.5 for the bisphosphine complex **1**, and a doublet signal at *δ* 202.7 ppm can be assigned for the monophosphine species generated in solution (see SI, Fig S9-12). The dynamic equilibrium has been studied in detail using CuI as phosphine scavenger[23] as well as by addition of excess PPh_3 to suppress the phosphine dissociation (see SI, Fig S16-28). HRMS (ESI$^+$) showed the peak for $[M-Cl]^+$ at m/z 1038.2220 (calculated for $C_{60}H_{49}Cl_2N_5P_2Ru$; 1038.2203) and the signal at 776.1379 for $[M-Cl-PPh_3]^+$.

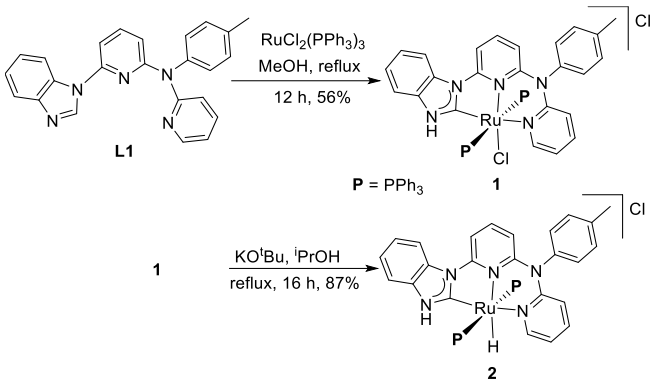

Scheme 2 Synthesis of Ru(II) pNHC complexes **1** and **2**

The metal-hydride complex [Ru(NNC^{H})(PPh$_3$)$_2$(H)]Cl, **2** was obtained in 87% yield as a yellow solid by reacting **1** with one equivalent KO^{t}Bu in isopropyl alcohol under reflux condition (Scheme 2). In contrast to **1**, the NMR spectrum of **2** indicates negligible phosphine dissociation in the solution. ^{1}H NMR spectrum of **2** shows a characteristic triplet at δ –10.55 ppm with $^{2}J_{P\text{-}H}$ = 23 Hz, showing the presence of the Ru–H functionality.[10,24] The ^{1}H NMR shows the presence of a singlet at δ 12.18 ppm for the protic N-H group and only one set of signals for the rest of the protons, as expected. The ^{31}P{^{1}H} NMR spectrum of **2** shows a signal at δ 51.18 ppm, which is shifted more downfield compared with complex **1** (δ 23.89 ppm) and also confirms that there was no phosphine dissociation.^{13}C{^{1}H} NMR spectrum shows the triplet signal for carbene carbon at δ 208.54 ppm. The FTIR spectrum of complex **2** displays a strong absorption at 1868 cm^{-1} assigned to metal hydride (Ru-H).[24a] In mass spectrometry, again, there is no phosphine dissociation observed. HRMS analysis showed a molecular ion peak for [M–Cl]$^{+}$ at m/z = 1004.2576. The molecular structures of complexes **1** and **2** have been confirmed by X-ray crystal diffraction studies**.** These are crystallized in an orthorhombic system with the Aea2 space group and a monoclinic system with the P2$_1$/c space group, respectively. The crystallographic parameters are given in Table S1, and selected bond lengths and angles are provided in Table S2-S3 (See SI). Figures 2 and 3 show the solid-state structures of complexes **1** and **2**, respectively.

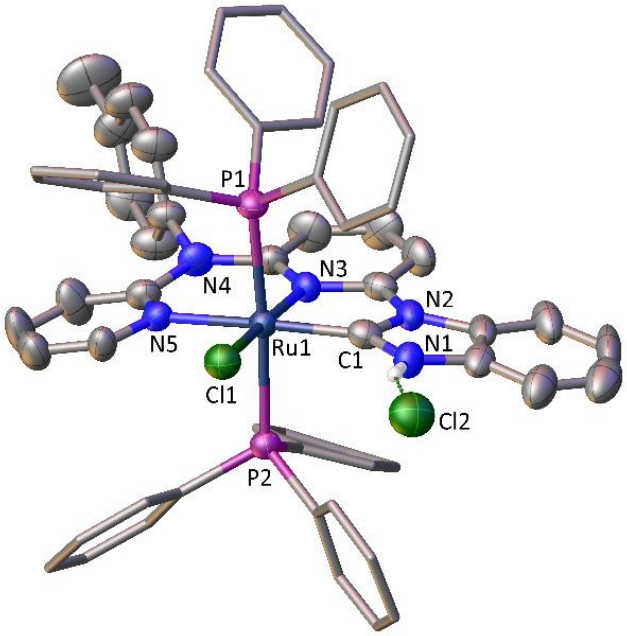

Figure 2 Solid-state structure of **1** (hydrogen atoms except for NH are omitted for clarity). Phenyl rings of phosphine ligand drawn in tube form for structure clarity. Selected bond lengths (Å) and bond angles (°): Ru1-C1 = 1.960(7), Ru1-N3 = 2.042(5), Ru1-N5 = 2.138(5), C1-N1 = 1.351(8), C1-N2 = 1.371(8) and N3-Ru1-N5 = 91.0 (2) C1-Ru1-N3 = 79.9(2), Cl1-Ru1-N5 = 94.4(1), C1-Ru1-N5 = 169.3(2).

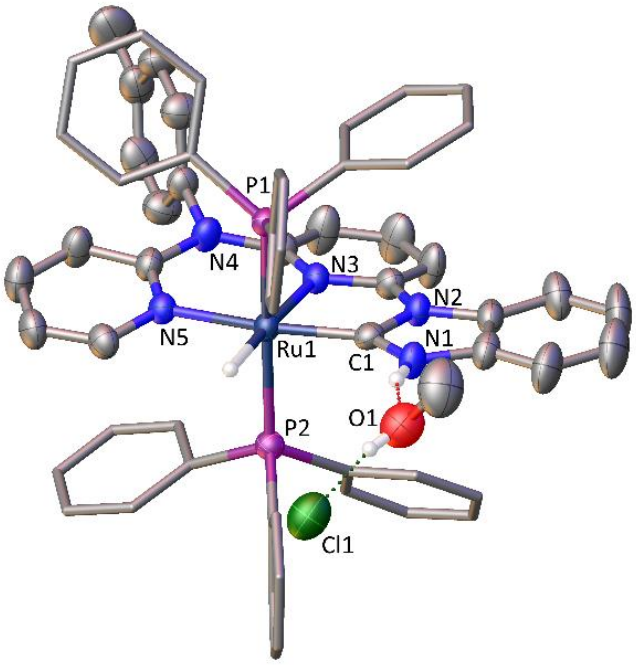

Figure 3 Solid-state structure of **2** (solvent molecules and hydrogen atoms except for NH, hydride are omitted for clarity). Phenyl rings of phosphine ligand drawn in tube form for structure clarity. Selected bond lengths (Å) and bond angles (º): Ru1-C1 = 1.949(3), Ru1-N3 = 2.115(3), Ru1-N5= 2.145(3), C1-N1 = 1.353(5), C1-N2 = 1.400(4) and N3-Ru1-N5 = 88.8(1), C1-Ru1-N3 = 79.4(1), C1-Ru1-N5 = 168.2(1).

The molecular structures of both **1** and **2** show the unsymmetrical NNC ligand around Ru bound as a tridentate pincer ligand forming a six-membered and a five-membered metallacycles. The two PPh_3 ligands are trans to each other, and one Cl^- (**1**) or H^- (**2**) ligands occupy the 6th coordination site. Ru-C and Ru-N distances in **1**, Ru1-C1 = 1.960(7), Ru1-N3 = 2.042(5), and Ru1-N5 = 2.138(5)) are comparable to the previously reported Ru(II) protic NHC complexes.[1f] One chloride counter ion is hydrogen bonded to the NH group of **1** with N–H···Cl distance of 2.395 Å with an angle of 153.74°. In the case of **2**, one molecule of a methanol solvent is found to be hydrogen bonded to the N-H group, while the Cl counterion is hydrogen bonded to the O-H of this methanol molecule.

Reversible deprotonation of 1 and 2

The reaction of complex **1** with one equiv of K_2CO_3 in dmso-d_6 solution led to no deprotonation of NH functionality of **1**. However, the equimolar reaction of complex **1** with Cs_2CO_3 in THF at ambient temperature led to the deprotonation of the pNHC complex to afford complex **1'** with 70% yield (Scheme 3). Similarly, the deprotonation of N-H functionality of **2** was carried out with Cs_2CO_3 in THF at room temperature with 75% yield. Alternatively, deprotonated metal hydride complex **2'** can be synthesized in 60% yield from the reaction of **2** with one equivalent of KO^{t}Bu in ^{i}PrOH at 80 °C for 6 h. Both **1'** and **2** react with aqueous HCl in methanol to give **1**, while **2'** reacts with aqueous HCl in methanol to give **2** and **1** in a stepwise manner. The protonation of the anionic NHC complexes **1'** and **2**' is also achieved by ammonium chloride (pKa = 9.24) in methanol, affording the pNHC complex **1**.

The formation of **1'** has been confirmed by NMR, Mass, and IR spectroscopy. ^{1}H NMR spectrum of **1'** in dmso-d_6 exhibits the disappearance of the NH signal at δ 14.15 and 13.97 ppm corresponding to complex **1**. ^{31}P{^{1}H} NMR spectrum of **1'** shows significant dissociation of phosphine ligand with peaks for metal bound phosphine at δ 48.26, 38.30 and 30.13 ppm along with free PPh_3 at -6.00 ppm. (See SI, Fig S37-40). The signals for two monophosphine species in solution (denoted as **1a'** and **1b'**) at δ 48.26 and 38.30 ppm may be due to two reasons; a) dmso-d_6 coordinated isomeric species having dmso-d_6 trans to PPh_3 ligand or trans to pyridine-N atom or b) chloride coordinated or dissociated forms. Since, ^{31}P{^{1}H} NMR of **1** shows only one monophosphine species, we are inclined to believe that isomeric monophosphine forms **1a'** and **1b'** are not due to different coordination sites of dmso-d_6 but due to chloride dissociation in **1'**. In the ^{13}C{^{1}H} NMR spectrum, the signal for the carbene carbon of deprotonated complex **1'** appears as a doublet at 195.26 ppm with $^2J_{CP}$ of 14.2 Hz, slightly up-field with respect to the corresponding signal at δ 202.74 ppm with $^2J_{CP}$ of 14.2 Hz for pNHC complex **1**. The slight upfield shift in the signal of deprotonated complex **1'** is in line with the previously reported anionic NHC complexes. The HRMS(ESI$^+$) analysis of complex **1'** in acetonitrile provides the two peaks at 1002.2445 for [M-Cl]$^+$ and 1043.2705 for [M+MeCN-Cl]$^+$, which agrees with the computed values: 1002.2439 and 1043.2735, respectively.

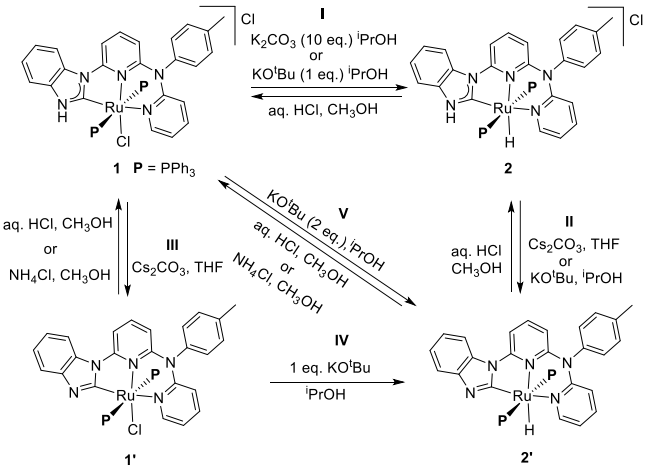

Scheme 3 Reversible *β*-deprotonation of **1** and **2** to synthesize **1'** and **2'**.

Similarly, the formation of **2'** was confirmed by the NMR, SCXRD, Mass, and IR spectroscopy. The ^{1}H NMR spectrum of **2'** in dmso-d_6 shows the doublets at δ 8.59 ppm correspond to ortho pyridyl proton slightly downfield from the complex **2** (doublet at δ = 8.27 ppm). ^{31}P{^{1}H} NMR spectrum of **2'** gives the information related to free phosphine at δ -6.00 and two signals at δ 57.53 and 54.80 ppm for monophosphine **(2a')** and bisphosphine **(2')** complexes, respectively. The ^{13}C{^{1}H} NMR of **2'** could not be obtained due to poor solubility. The FTIR spectrum of complex **2'** displays a strong absorption at 1885 cm^{-1} assigned to metal hydride (Ru-H) (See SI Fig S51).

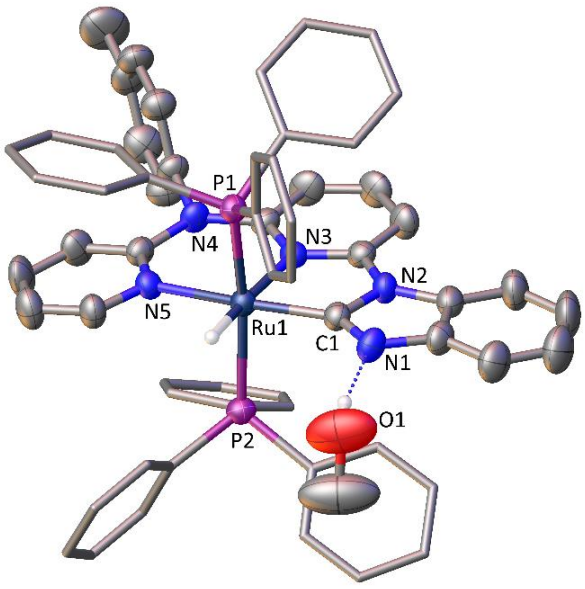

Figure 4 Solid-state structure of **2'** (solvent molecules and hydrogen atoms except for methanol OH are omitted for clarity). Phenyl ring of phosphine ligand are drawn in tube form for structure clarity. Selected bond lengths (Å) and bond angles (°): Ru1-C1 = 1.971(3), Ru1-N3 = 2.112(2), Ru1-N5 = 2.136(2), C1-N1 = 1.326(3), C1-N2 = 1.443(3) and C1-Ru1-N3 = 80.9(1), C1-Ru1-N5 = 170.2(9), N3-Ru1-N5 = 89.7(9).

The molecular structure of complex **2'** consists of a ruthenium center in a distorted octahedral environment with NNC mer-tridentate chelating ligand. The two PPh_3 are trans to each other, and hydride is trans to pyridine. We have compared the protic complex **2** with deprotonated **2'** by looking more closely at the bond lengths. **2'** shows a slightly shorter bond length for N1-C1 compared to **2**, i.e., N1-C1(1.326(3) Å vs. 1.353 (5)) Å, thus indicating a partial double bond character. Similarly, the N2-C1 bond length of **2'** (N2-C1 = 1.443(3) Å) is slightly longer compared to **2** (N2-C1 = 1.400(4) Å) as expected.

Cooperative bond activations using 1'

The $^{13}C\{^1H\}$ NMR of **1'** shows an upfield shift of 7.4 ppm in the chemical shift value of carbene carbon (δ 195.3 ppm) compared to **1** (δ 202.7). Similar upfield shifts in the carbene carbon of pNHC complexes after deprotonation have been reported in the literature and discussed as an anionic-naked-NHC ligand.[2c,11b,25] The deprotonated nitrogen atom is expected to be a basic site and can participate in the metal-ligand cooperativity. To check the cooperative reactivity of anionic NHC complexes, we have performed some model reactions that can provide insight into the chemical reactivity typically used to describe the cooperative bond activation of small molecules (Scheme 4).

Complex **1'** shows the ability to induce heterolytic chevage of the H-H bond of the dihydrogen and gives the pNHC-Ru-hydride complex **2**. The treatment of complex **1'** in dmso-d_6 solution with hydrogen gas at 80 °C (1 atm) or room temperature (10 bar) led to the formation of complex **2**, which was confirmed by multinuclear NMR spectroscopy. Further, the anionic NHC has been shown to polarize the hydrogen of the sp carbon centre of phenylacetylene.[26] The reaction of phenylacetylene with **1'** in dmso-d_6 at 80 °C leads to the formation of the acetylide complex **6**. Spectroscopic analysis suggests that complex **6** shows some degree of dissociation of PPh_3 from the protic NHC acetylide adduct. The ^1H NMR resonances at δ 13.52 and 13.93 ppm are attributed to the NH proton of bisphosphine complex **6** and the in situ generated monophosphine species **6a**, respectively. The $^{31}P\{^1H\}$ spectrum shows three signals. The signal associated with complex **6** resonates at δ 32.43 ppm, and the monophosphine species **6a** detected at δ 49.00 ppm along with the signal for free phosphine at δ -6.00 ppm. In HRMS, the isotropic distribution pattern of complex **6** was consistent with the simulated pattern for $[M\text{-}Cl]^+$ at m/z = 1104.2911.

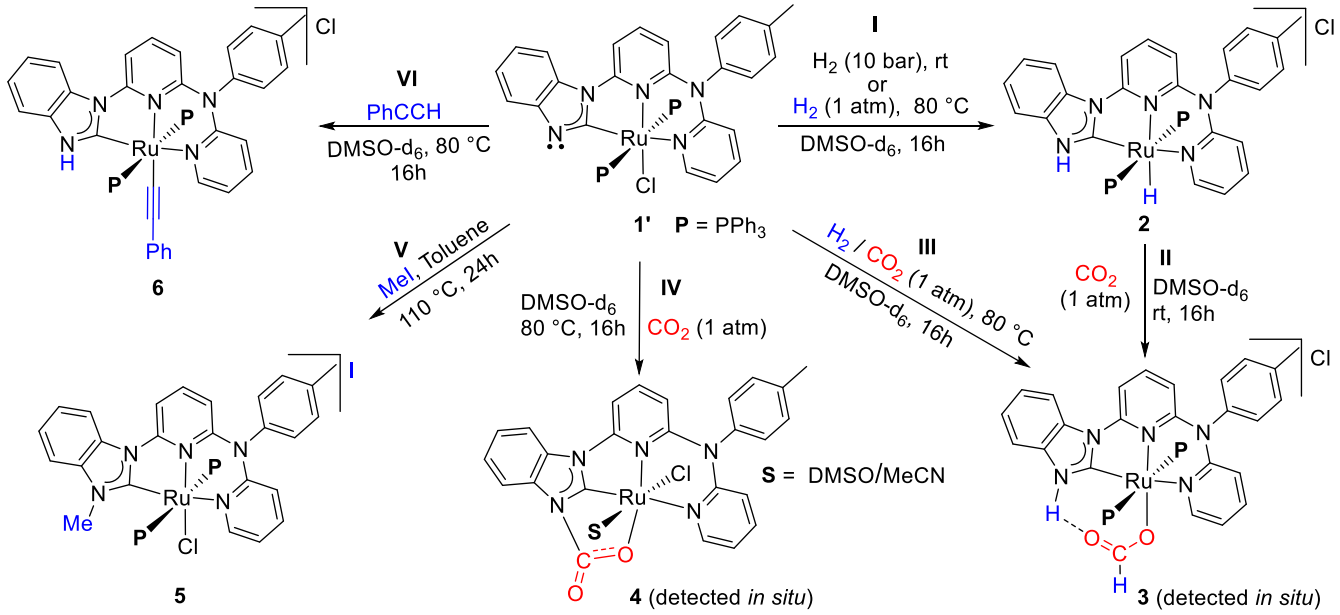

Scheme 4 Cooperative bond activations of small molecules using **1'**.

To investigate the ability of the anionic NHC complex in CO_2 capture, an NMR tube experiment was performed. The $^{31}P\{^1H\}$ NMR spectrum of the CO_2 capture reaction indicates a significant peak for the free phosphine ligand while signals of the starting complex **1'** almost disappeared. One small peak at δ 25.19 ppm is observed which has been confirmed to not be of $O{=}PPh_3$. This may be for some Ru species generated in small amount due to decomposition. Also, both $^{13}C\{^1H\}$ NMR and ESI^+-MS indicate no phosphine containing species for the CO_2 captured complex **4**. The $^{13}C\{^1H\}$ NMR spectrum exhibits loss of a doublet signal at δ 195.26 ppm ($^2J_{CP}$ = 14.2 Hz), and the appearance of a new singlet at δ 193.34 ppm attributed to the absence of coordinated phosphine co-ligand (Figure 5). A new singlet peak at δ 155.50 ppm is assigned as CO_2 bound with Ru/N Lewis pair of complex **1'**. The in situ generated CO_2 captured species is spectroscopically analyzed as complex **4** with the help of $^{13}C\{^1H\}$ NMR and ESI^+-MS. The mass spectrometry (ESI^+) shows a signal at m/z = 598.1032 for $[M+MeCN\text{-}DMSO]^+$, m/z = 616.1129 for $[M+MeCN+H_2O\text{-}DMSO]^+$ and at m/z = 682.1561 for $[M+(2MeCN)+(DMSO)\text{-}Cl]^+$ attributable to fragments originating from **4**.

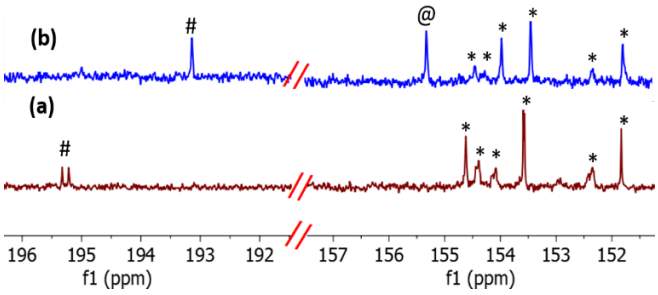

Figure 5 $^{13}C\{^1H\}$ NMR spectra of CO_2 activation by anionic NHC complex in dmso-d_6. (a) The spectrum before bubbling with CO_2; *: Peak from complex **1'**; #: doublet peak of carbene from complex **1'** (b) The spectrum after bubbling CO_2 gas; @: peak from bound CO_2 (complex **4**); #: new carbene singlet signal for complex **4**; *: other signals for complex **4**.

To gain insight into the hydrogenation of CO_2, a solution of **1'** in dmso-d_6 was treated with an approximate 2:1 mixture of H_2 and CO_2. After 16 h at 80 °C, this led to the conversion of **1'** to formate complex **3** (See SI, Fig S70-73). A peak at δ 8.58 ppm appeared in the ^1H NMR spectrum of the solution in dmso-d_6, indicating the presence of the formate product (HCO_2^-) as shown in Figure 6. Based on the reported literature,[27] CO_2 hydrogenation can be explained to proceed via the metal hydride complex, **2**. The ^1H NMR spectroscopy showed a distinctive signal at δ -10.56 ppm, validating the production of the Ru-H species from the interaction of **1'** with H_2 in dmso-d_6. The $^{31}P\{^1H\}$ signal at δ 51.92 ppm also supports the existence of Ru-H species complex **2** in the reaction mixture.

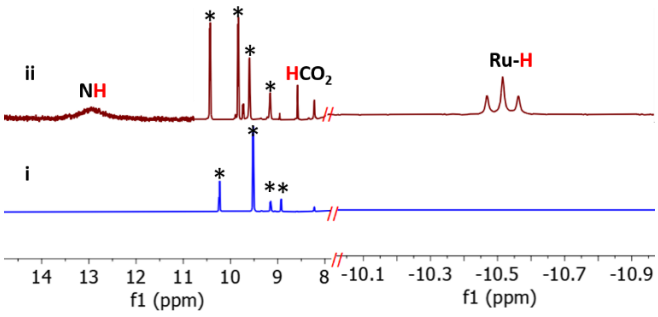

Figure 6 ^1H NMR spectrum of CO_2 hydrogenation to formate by anionic NHC complex in dmso-d_6. (i) The spectrum before bubbling with CO_2 and H_2 mixture; *: peaks from complex **1'** (ii) The spectrum after bubbling CO_2 and H_2 gas.

Anionic NHC complex **1'** proved to be a precursor for synthesizing classical NHC complex **5** via heterolytic cleavage of alkyl halide. The reaction of complex **1'** with 1.5 equivalent of iodomethane in toluene led to the formation of a corresponding classical NHC complex **5**. The ^1H NMR shows two methyl singlets at δ = 4.52 and 2.46 ppm for N-methyl benzimidazole and methyl proton of the p-tolyl group of the ligand, respectively. The $^{31}P\{^1H\}$ NMR spectrum illustrates the phosphine signal detected at δ 31.48 ppm. In addition, the $^{13}C\{^1H\}$ NMR spectrum showed characteristic resonance of carbene carbon appearing at δ 205.76 ppm and N-Me signal at δ 39.65 ppm. The mass spectrometry analysis shows m/z calculated for $C_{61}H_{51}ClN_5P_2Ru$ $[M\text{-}I]^+$ 1052.2359, found 1052.2381, and a signal at m/z calcd for $C_{43}H_{36}ClN_5PRu$ $[M\text{-}I\text{-}PPh_3]^+$ 790.1443, found 790.1460 related to complex **5** (See SI, Fig S74-79).

Computational analysis

Computational calculations were performed using the ORCA 5.0.3 program, and r^{2}SCAN-3c composite functional,[28] was used for the optimization of complexes **1, 2, 1'** and **2'**. The optimized geometries of complexes show excellent agreement with the experimental values (Single crystal X-ray diffraction data). Therefore, r^{2}SCAN-3c composite functional is acceptable as a reliable method for predicting the covalent geometry of these complexes. The electrostatic potential near the deprotonated nitrogen for complexes **1'** and **2'** exhibit a distinct negative maximum (Figure 7). In both the complexes, the phenyl rings of the triphenylphosphine ligands partially shield the basic nitrogen centre. Figures 8 and 9 show the comparison of DFT optimized geometries of compounds **1** with **1'** and **2** with **2'**, respectively. The optimized geometry of complex **1'** exhibits a slight shortening of C1-N1(1.324 Å) and slight lengthening in the C1-N2 (1.433 Å) bond in comparison to complex **1** as observed in the optimized structure of **2'**.

The natural population analysis (NPA) calculation was performed on the optimized structures of **1**, **1'**, **2**, and **2'** using JANPA. While NPA analysis indicates a greater electron density at the N-atoms of the carbene ligands in all complexes, a comparison between pNHC complexes **1** and **2** with their β-deprotonated analogues **1'** and **2'** shows the accumulation of increased electron density at N1, a little less at N2, and only a small increase at C1 compared to the protic NHC complexes. As shown in Figure 8, the nitrogen (N1) of β-deprotonated NHC complex **1'** has a major difference (-0.054 C) in the calculated atomic charge in comparison to carbene carbon (C1) (-0.009 C). Similarly, the charge distribution in **2'** in Figure 9 reveals the appearance of a larger net negative charge (-0.056 C) at nitrogen(N1) and slightly less charge (-0.026 C) accumulated on nitrogen (N2) compared to carbene carbon (C1) (-0.009 C) with respect to protic NHC complex **2**. The high electronic charge on the nitrogen (N1) of **1'** and **2'** further supports these complexes having anionic-naked-NHC ligands.

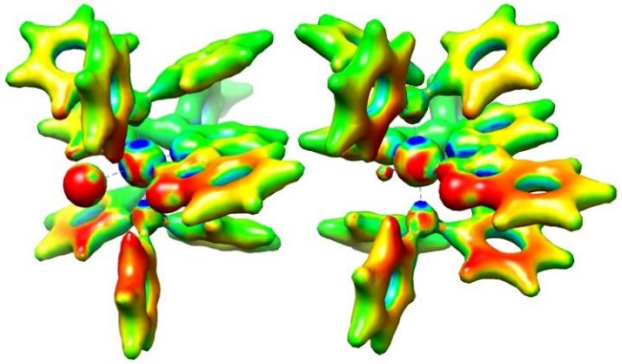

Figure 7 Electrostatic potential map of the isodensity surface (0.14 a.u.) of complex **1'** (left) and **2'** (right) in the range -0.09 (red) to 0.09 a.u. (blue).

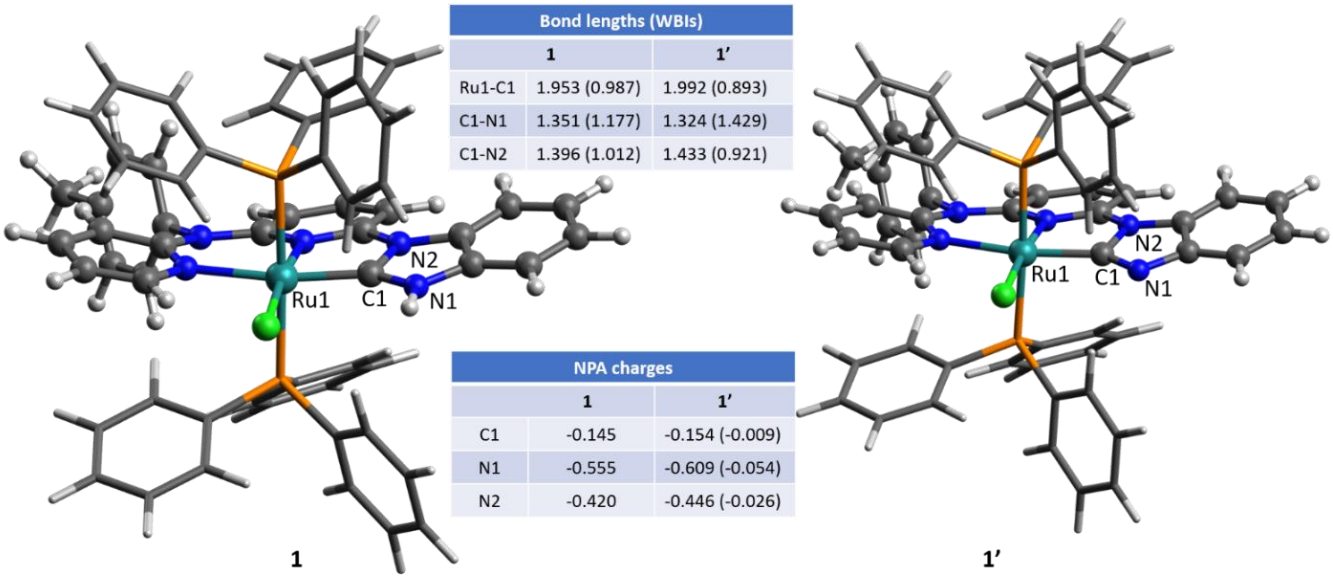

Figure 8 DFT optimized structures of **1** and **1'** (PPh_3 ligands are shown as sticks for clarity). Relevant bond lengths (Å), Wiberg Bond Indices and NPA charges are shown in tables for comparison.

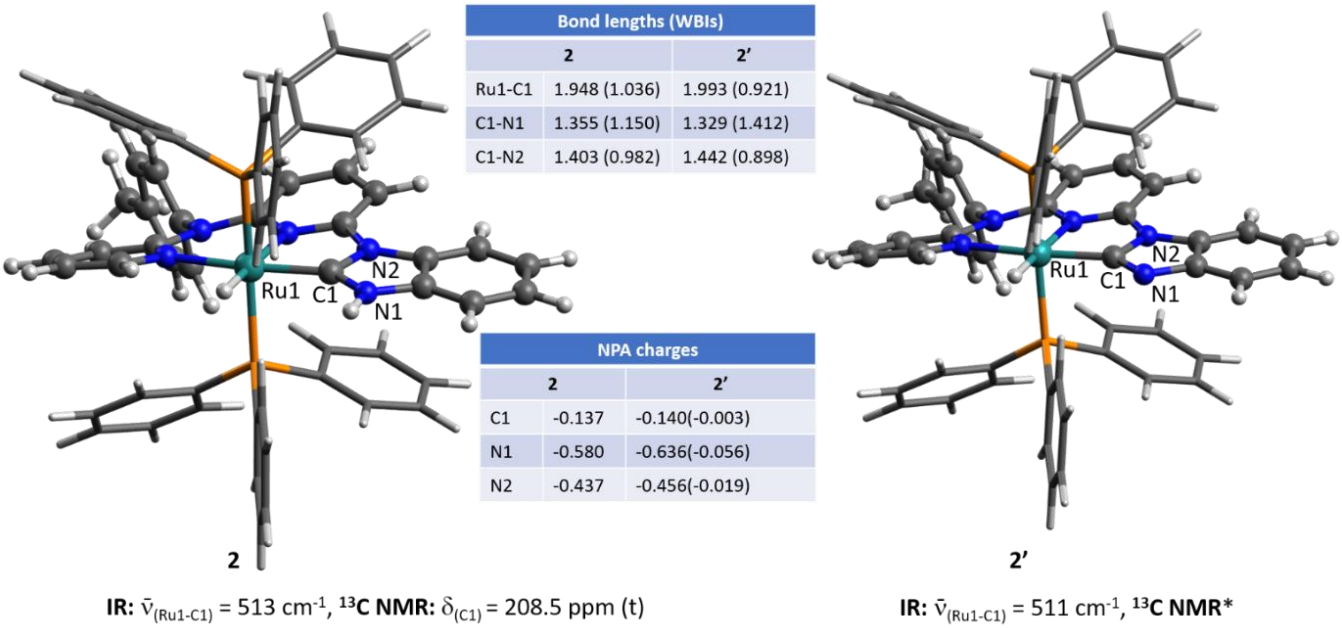

Figure 9 DFT optimized structures of **2** and **2'** (PPh_3 ligands are shown as sticks for clarity). Relevant bond lengths (Å), Wiberg Bond Indices and NPA charges are shown in tables for comparison. * ^{13}C {^{1}H} NMR could not be obtained due to poor solubility.

Conclusion

In summary, we have synthesized a set of Protic and β-deprotonated N-heterocycle carbene Ru (II) complexes **(1-2)** and (**1'-2'**) with an unsymmetrical NNC ligand. The spectroscopic and theoretical evaluations were used to gain insight into the electronic structures. The NPA calculations provide reliable information related to the charge distribution in the protic and β-deprotonated Ru(II) NHC complexes. The experimental and computational investigation suggests the maximum electronic charge accumulation on the *β*-deprotonated nitrogen (N1) compared to the carbene carbon (C1) of Ru(II) NHC complexes and, therefore, complexes **1'** and **2'** are best described as having anionic-naked-NHC ligand. The protonation of **1'** and **2'** by

reaction with NH_4Cl in methanol led to the formation of their respective protic NHC complexes. We have explored the cooperative small molecule activation reactivity of **1'** with the activation of H-H, C(sp^3)-I, and C(sp)-H bonds of the hydrogen molecule, iodomethane, and terminal alkyne, respectively. CO_2 capture and its reduction to formate have also been described at ambient temperature and mild pressure. The combined effect (Lewis acid and Lewis base) of the Ru/N couple of anionic NHC can be described as a cooperative small molecule activation. Further applications of these complexes in various catalytic reactions are under investigation.

Experimental Section

General considerations

All reactions were performed in oven-dried glassware under an inert atmosphere using MBraun glovebox and standard Schlenk or high vacuum line techniques. All reagents and solvents were purchased from commercial sources. THF, Et_2O, and toluene were refluxed over sodium benzophenone ketyl and distilled under a nitrogen atmosphere prior to use. The ruthenium precursor $[RuCl_2(PPh_3)_3]$ was synthesized according to reported procedure[29] and stored under a nitrogen atmosphere. Deuterated solvents ($CDCl_3$, DMSO-d_6) were purchased from Eurisotop and Sigma-Aldrich and distilled over calcium hydride. NMR samples of sensitive compounds were prepared in the glovebox under a nitrogen atmosphere. NMR spectra were recorded at room temperature on a Bruker Avance-400 and 500 NMR spectrometer. Chemical shifts were reported relative to residual solvent peaks of the respective deuterated solvents. IR spectra were recorded on Bruker alpha II compact FTIR IR spectrometer. Electrospray ionization mass spectra (ESI-MS) and high-resolution mass spectra (HRMS) measurements were performed on a Bruker-Doltonics-micro TOF -QII spectrometer at 22 °C.

Synthesis and characterization

Synthesis of Ligand L1: An oven-dried 100 ml 2-neck R.B. flask, fitted with a reflux condenser was charged with 1-(6-bromopyridin-2-yl)-1*H*-benzo[*d*]imidazole, **a** (2.740 g, 10 mmol), 2-(p-tolyl) pyridine, **b** (2.392 g, 13 mmol), $Pd(dba)_2$ (0.348 g, 0.38 mmol), dppf (0.205 g, 0.37 mmol), sodium tert-butoxide (1.150 g, 12 mmol) and anhydrous toluene (20 mL) under inert atmosphere. The flask was lowered into an oil bath and heated to reflux for 24 h. After cooling to room temperature, ethyl acetate (20 ml) was added and stirred for 30 min at room temperature when a red-colored precipitate was formed. The reaction mixture was filtered through celite, the red precipitate was discarded, and the filtrate was evaporated under reduced pressure on a rotary evaporator to get a brown solid. The crude product was purified by column chromatography on silica gel with ethyl acetate/hexane (70:30) to give a 2.489 g light brown product (yield- 66%). **^{1}H NMR** (400 MHz, $CDCl_3$ 25 °C) δ 8.42 – 8.39 (m, 2H), 7.76 (d, *J* = 8.0 Hz, 1H), 7.69 (t, *J* = 8.0 Hz, 1H), 7.64 – 7.52 (m, 2H), 7.31 – 7.24 (m, 3H), 7.20 (t, *J* = 8.3 Hz, 2H), 7.13 – 6.98 (m, 5H), 2.42 (s, 3H). **^{13}C{^{1}H} NMR** (100 MHz, $CDCl_3$, 25 °C) δ 157.8, 157.5, 148.6, 144.6, 141.8, 141.1, 139.9, 137.9, 136.6, 132.2, 130.8, 128.3, 123.8, 123.0, 120.3, 119.0, 118.2, 114.0, 112.0, 105.5, 21.3. **DEPT-135 NMR** (126 MHz, $CDCl_3$) δ 148.5, 141.0, 139.8, 137.8, 130.7, 128.3, 123.7, 123.0, 120.2, 119.0, 118.1, 113.9, 111.9, 105.4, 21.2. HRMS (ESI^+) m/z calcd for $C_{24}H_{19}N_5$ $[M+H]^+$ 378.1713, found 378.1722. Anal. Calcd for $C_{24}H_{19}N_5$: C, 76.37; H, 5.07; N, 18.55. Found: C, 76.12; H, 5.04; N, 18.48.

Synthesis of 1: An oven-dried Schlenk tube was charged with **L1** (0.075 g, 0.2 mmol) in methanol (10 mL), followed by the addition of $RuCl_2(PPh_3)_3$ (0.191 g, 0.2 mmol). The resulting mixture was stirred at reflux temperature for 12 h. After the completion of the reaction, the mother liquor was filtered through a short celite pad and reduced to 1-2 mL at reduced pressure; then, diethyl ether was added, and the yellow precipitate was obtained. Finally, after drying in a high vacuum, the compound was obtained as a yellow powder. Yield 0.120 g (56%).**^{1}H NMR** (500 MHz, DMSO-d_6, 25 °C) δ 14.15 (s, 1H), 13.97 (s, 1H), 9.35 (d, *J* = 6.0 Hz, 1H), 9.07 (d, *J* = 5.8 Hz, 2H), 8.13 (d, *J* = 8.2 Hz, 1H), 7.86 (d, *J* = 8.2 Hz, 2H), 7.75 (d, *J* = 8.1 Hz, 1H), 7.72 – 7.65 (m, 2H), 7.60 (d, *J* = 7.0 Hz, 2H), 7.52 (t, *J* = 7.9 Hz, 6H), 7.36 (d, *J* = 8.9 Hz, 10H), 7.25 (d, *J* = 7.9 Hz, 6H), 7.20 (q, *J* = 9.1 Hz, 9H), 7.12 (d, *J* = 8.1 Hz, 7H), 7.08 (d, *J* = 17.1 Hz, 19H), 6.84 (t, *J* = 6.5 Hz, 1H), 6.75 (d, *J* = 7.6 Hz, 3H), 6.52 (d, *J* = 8.9 Hz, 1H), 6.25 (d, *J* = 9.6 Hz, 2H), 6.12 (d, *J* = 8.9 Hz, 2H), 5.75 (d, *J* = 7.6 Hz, 2H), 2.45 (s, 6H). **^{31}P{^{1}H} NMR** (202 MHz, DMSO-d_6, 25 °C) δ 32.44 (s), 23.89(s), -6.00(s, PPh_3). **^{13}C{^{1}H} NMR** (126 MHz, DMSO-d_6, 25 °C) (Ru-$C_{Carbene}$) δ 204.5 (t, *J* = 12.4 Hz), (Ru-$C_{Carbene}$) 202.8 (d, *J* = 14.2 Hz), 154.0, 153.5, 153.5, 153.0, 152.8, 152.8, 152.7, 140.4, 139.6, 139.5, 138.72, 137.9, 135.9, 133.3, 133.2, 133.1, 132.7, 132.7, 132.6, 132.5, 132.3, 132.0, 132.0, 131.5, 131.4, 131.2, 131.1, 130.9, 130.8, 130.6, 130.5, 130.2, 129.8, 129.7, 129.3, 129.2, 128.7, 128.7, 128.6, 128.1, 128.0, 128.0, 127.9, 127.9, 124.4, 123.4 122.8, 117.6, 117.0, 113.2, 112.0, 111.7, 111.3, 111.2, 105.6, 105.6, 20.8, 20.7.**DEPT-135 NMR** (126 MHz, DMSO-d_6, 25 °C) δ 152.6, 151.6, 138.5, 137.6, 137.2, 136.1, 133.1, 132.9, 132.5, 132.4, 132.4, 132.3, 132.0, 131.7, 131.7, 131.2, 131.1, 129.6, 129.4, 129.1, 129.0, 129.0, 128.5, 128.5, 128.4 (d, *J* = 2.3 Hz), 127.9, 127.8, 127.7, 127.7, 127.7, 124.2, 123.8, 123.1, 122.5, 117.4, 117.0, 116.8, 113.0, 112.0, 111.8, 111.5, 111.0, 110.9, 105.4, 105.3, 20.5, 20.5. **ATR-FTIR (solid):** ῡ cm^{-1} (Ru-$C_{carbene}$) = 517. HRMS (ESI^+) m/z calcd for $C_{60}H_{49}Cl_2N_5P_2Ru$ $[M-Cl]^+$ 1038.2203, found 1038.2220. Anal. Calcd for $C_{60}H_{49}Cl_2N_5P_2Ru$: C, 67.10; H, 4.60; N, 6.52. Found: C, 67.48; H, 4.30; N, 6.82.

Synthesis of 2. Complex **1** (0.053 g, 0.05 mmol) was dissolved in isopropyl alcohol in a Schlenk tube. Then, potassium tert-butoxide (0.005 g, 0.05 mmol) was added, stirred, and refluxed for 18 h. After completing the reaction, a yellow precipitate was obtained. After slow cooling, the solution was filtered off, and the yellow solid was washed several times with Et_2O. The complex was obtained as a bright yellow-orange powder. Yield: 0.045 g (87%). **^{1}H NMR** (500 MHz, DMSO-d_6, 25 °C) δ 12.18 (s, 1H), 8.28 (d, *J* = 6.3 Hz, 1H), 7.68 (t, *J* = 8.4 Hz, 1H), 7.57 (d, *J* = 8.4 Hz, 1H), 7.45 (d, *J* = 8.1 Hz, 2H), 7.39 (d, *J* = 3.7 Hz, 2H), 7.24 (s, 0H), 7.17 – 7.08 (m, 9H), 7.05 (t, *J* = 7.6 Hz, 14H), 6.71 (d, *J* = 7.9 Hz, 2H), 6.31 (d, *J* = 8.4 Hz, 1H), 6.02 (t, *J* = 6.5 Hz, 1H), 5.84 (d, *J* = 9.0 Hz, 1H), 2.43 (s, 3H), -10.55 (t, *J* = 23.0 Hz, 1H). **^{31}P{^{1}H} NMR** (202 MHz, DMSO-d_6, 25 °C) δ 51.18. **^{13}C{^{1}H} NMR** (126 MHz, DMSO-d_6, 25°C) δ 208.5 (Ru-$C_{Carbene}$),156.0,154.7,152.8,150.7,140.8,139.7,136.6,134.4,134.3,134.1,133.8,133.6,132.9,132.8,132.8,132.6,132.0,131.9,130.3,129.8,128.3,123.4,122.1,117.4,116.7, 111.8, 111.0, 110.3, 105.9, 21.2. **ATR-FTIR (solid):** ῡ cm^{-1} (Ru-$C_{carbene}$) = 513 and ῡ cm^{-1} (Ru-H) = 1868. HRMS (ESI^+) m/z calcd for $C_{60}H_{50}P_2ClRuN_5$ $[M-Cl]^+$1004.2596, found 1004.2576. Anal Calcd for $C_{60}H_{50}ClN_5P_2Ru$: C, 69.32; H, 4.85; N, 6.74. Found: C, 69.01; H, 4.53; N, 6.61.

Synthesis of 1': In a glovebox, an oven-dried 15 mL vial equipped with a magnetic stirring bar was charged with complex **1** (0.118 g, 0.11 mmol) and cesium carbonate (0.035 g, 0.11 mmol) in dry THF. The mixture was stirred overnight at room temperature. After completion of the reaction, the yellow residue was filtered and washed several times with Et_2O to obtain a yellow powder. Yield: 0.080 g (70%). **^{1}H NMR** (500 MHz, DMSO-d_6, 25 °C) δ 10.23 (d, *J* = 5.9 Hz, 1H), 9.51 (d, *J* = 7.6 Hz, 1H), 7.78 (d, *J* = 8.2 Hz, 2H), 7.55 (t, *J* = 8.4 Hz, 2H), 7.51 (d, *J* = 7.1 Hz, 2H), 7.46 – 7.39 (m, 13H), 7.38 – 7.34 (m, 16H), 7.30 (t, *J* = 8.1 Hz, 13H), 7.27 – 7.20 (m, 12H), 7.15 (t, *J* = 7.5 Hz, 5H), 7.13 – 7.08 (m, 3H), 7.05 (t, *J* = 8.9 Hz, 4H), 7.00 (t, *J* = 7.0 Hz, 7H), 6.86 (t, *J* = 8.9 Hz, 8H), 6.72 (t, *J* = 6.5 Hz, 2H), 6.48 (d, *J* = 8.6 Hz, 2H), 6.37 (d, *J* = 8.8 Hz, 2H), 6.19 (d, *J* = 8.4 Hz, 1H), 6.13 (d, *J* = 8.6 Hz, 2H), 2.42 (s, 3H), 2.39 (s, 3H). **^{31}P NMR** (202 MHz, DMSO-d_6, 25 °C) δ 47.81, 38.30, 30.13 -5.99. **^{13}C{^{1}H} NMR** (126 MHz, DMSO-d_6, 25 °C) δ 195.3 (Ru-$C_{Carbene}$) (d, *J* = 14.2 Hz), 154.6, 153.6 (d, *J* = 2.8 Hz), 151.8, 148.6, 141.8, 138.7, 138.5, 137.2, 133.9, 133.4, 133.2, 133.1, 132.9 (d, *J* = 9.2 Hz), 132.3 132.1 (d, *J* = 2.8 Hz), 131.5 (d, *J* = 10.1 Hz), 130.3, 129.1, 128.8 (d, *J* = 2.3 Hz), 128.8 (d, *J* = 2.8 Hz), 127.7 (d, *J* = 9.2 Hz), 122.0, 119.4, 117.9, 116.3, 115.6, 111.1, 110.1, 101.7, 20.8. **DEPT-135 NMR** (126 MHz, DMSO-d_6, 25 °C) δ 154.4, 152.2, 138.3, 136.9, 136.1,

133.1 (d, *J* = 6.2 Hz), 132.9, 132 7 (d, *J* = 9.6 Hz), 131.8 (d, *J* = 3.4 Hz), 131.6, 131.3 (d, *J* = 6.2 Hz), 131.2, 130.0, 129.2, 128.8 (d, *J* = 7.3 Hz), 128.7-128.4 (m), 127.5 (d, *J* = 8.5 Hz), 127.0 (d, *J* = 8.5 Hz), 121.7, 121.2, 119.2, 118.5, 117.7, 116.9 – 115.7 (m), 115.3, 110.8, 109.9, 109.5, 109.21, 101.9, 101.4, 31.0, 20.5. **ATR-FTIR (solid):** ῡ cm^{-1} (Ru-$C_{carbene}$) = 513. HRMS (ESI^+) m/z calcd for $C_{60}H_{48}ClN_5P_2Ru$ $[M\text{-}Cl]^+$ 1002.2439, found 1002.2445. Anal. Calcd for ($C_{60}H_{48}ClN_5P_2Ru$ + CsCl): C, 59.76; H, 4.01; N, 5.81. Found: C, 59.38; H, 4.16; N, 5.89.

Synthesis of 2'. Complex **2** (0.118 g, 0.11 mmol) and cesium carbonate (0.035 g, 0.11 mmol) was suspended in dry THF (5 mL) in an oven-dried 15 mL vial equipped with a magnetic stirring bar. The reaction was stirred at room temperature overnight. After the completion of the reaction, a yellow precipitate appeared. The yellow solid was washed with diethyl ether (3x5 mL) to afford the desired product. Yield: 0.025 g (75%). **^{1}H NMR** (500 MHz, DMSO-d_6, 25°C) δ 8.59 (d, *J* = 3.5 Hz, 1H), 7.56 (d, *J* = 7.9 Hz, 4H), 7.40 (d, *J* = 4.7 Hz, 9H), 7.32 (t, *J* = 8.8 Hz, 2H), 7.25 – 7.21 (m, 8H), 7.19 (t, *J* = 8.3 Hz, 8H), 7.13 (t, *J* = 7.2 Hz, 4H), 7.07 (t, *J* = 7.1 Hz, 4H), 6.99 (t, *J* = 6.8 Hz, 5H), 6.94 (t, *J* = 8.1 Hz, 7H), 6.81 (s, 1H), 6.35 (t, *J* = 6.4 Hz, 2H), 6.28 (d, *J* = 8.8 Hz, 2H), 6.23 (d, *J* = 8.5 Hz, 2H), 2.41 (s, 6H). **^{31}P{^{1}H} NMR** (202 MHz, DMSO, -d_6, 25 °C) δ 57.53, 54.80, -6.00. **ATR-FTIR (solid):** ῡ cm^{-1} (Ru-$C_{carbene}$) = 511 and ῡ cm^{-1} (Ru-H) = 1885. HRMS (ESI^+) m/z calcd for $C_{60}H_{49}ClN_5P_2Ru$ $[M+H]^+$ 1004.2596, found 1004.2617. Anal. Calcd for ($C_{60}H_{49}N_5P_2Ru$ + KCl): C, 66.87; H, 4.58; N, 6.50. Found: C, 66.95; H, 4.81; N, 6.89.

Heterolytic cleavage of H_2 (1 atm) at 80 °C by 1'. In a N_2 glove box, J. Young NMR tube was charged with complex **1'** (50 mg, 0.048 mmol) and DMSO-d_6, then NMR was recorded. This solution was bubbled with hydrogen gas while it was heated for two hours at 80 °C. This step was followed by closing the NMR tube under an H_2 environment and heating it at 80 °C overnight. **^{1}H NMR** (400 MHz, DMSO-d_6, 25°C) δ 12.26 (s, 1H), 8.26 (d, *J* = 6.1 Hz, 2H), 7.67 (t, *J* = 8.4 Hz, 2H), 7.56 (d, *J* = 8.4 Hz, 2H), 7.14 (d, *J* = 7.0 Hz, 7H), 7.10 (d, *J* = 4.4 Hz, 16H), 7.06 (d, *J* = 7.5 Hz, 18H), 6.69 (d, *J* = 8.1 Hz, 4H), 6.29 (d, *J* = 8.7 Hz, 2H), 6.02 (t, *J* = 6.5 Hz, 2H), 5.82 (d, *J* = 8.9 Hz, 2H), -10.57 (t, *J* = 22.9 Hz, 1H). **^{31}P{^{1}H} NMR** (202 MHz, DMSO-d_6, 25°C) δ 51.12.

Heterolytic cleavage of H_2 (10 bar) at room temperature by 1'. In a high-pressure reactor, a Poly tetra fluoroethylene (PTFE) tube was charged with complex **1'** (50 mg, 0.048 mmol) and DMSO-d_6 (0.5 mL), applied 10 bar H_2 pressure, and stirred at ambient temperature for 18 h. After that solution was transferred into an NMR tube, and ^{1}H and ^{31}P{^{1}H} were recorded. **^{1}H NMR** (500 MHz, DMSO-d_6, 25 °C) δ 12.27 (s, 1H), 8.68 (s, 1H), 8.26 (s, 1H), 7.70 – 7.55 (m, 7H), 7.43 (d, *J* = 7.4 Hz, 14H), 7.38 – 7.32 (m, 8H), 7.19 – 7.09 (m, 20H), 7.09 – 6.92 (m, 13H), 6.70 (d, *J* = 7.9 Hz, 5H), 6.28 (s, 1H), 5.83 (d, *J* = 9.0 Hz, 1H), 2.42 (s, 20H), -10.56 (t, *J* = 23.0 Hz, 1H), -11.62 (d, *J* = 27.1 Hz, 2H). **^{31}P{^{1}H} NMR** (202 MHz, DMSO-d_6, 25°C) δ 51.17.

CO_2 hydrogenation by 2. In a glovebox under a nitrogen atmosphere, a J. young NMR tube was charged with complex **2** (50 mg, 0.048 mmol) in 0.5 mL DMSO-d_6. J. young NMR tube was taken out from the glovebox, and the NMR tube was purged with CO_2 to ensure a complete CO_2 environment in the NMR tube. Then, the NMR tube was closed under the CO_2 environment and left overnight at room temperature. NMR spectroscopy was used to analyze product **3** as the formate peak was assigned at δ 8.56 ppm. **^{1}H NMR** (500 MHz, **DMSO-d_6, 25 °C)** δ 12.35 (s, 1H), 9.70 (dd, *J* = 5.8, 2.1 Hz, 1H), 8.56 (s, 0.09H), 8.26 (d, *J* = 6.0 Hz, 1H), 7.98 (d, *J* = 7.9 Hz, 1H), 7.88 (d, *J* = 8.2 Hz, 1H), 7.64 (d, *J* = 8.4 Hz, 1H), 7.49 (d, *J* = 8.4 Hz, 2H), 7.45 (d, *J* = 8.2 Hz, 2H), 7.40 (d, *J* = 8.1 Hz, 5H), 7.35 (t, *J* = 7.4 Hz, 9H), 7.28 (t, *J* = 7.8 Hz, 11H), 7.15 (t, *J* = 6.6 Hz, 6H), 7.10 (d, *J* = 3.5 Hz, 2H), 7.05 (t, *J* = 7.6 Hz, 15H), 6.92 (d, *J* = 8.5 Hz, 1H), 6.86 (s, 0H), 6.70 (d, *J* = 8.2 Hz, 2H), 6.65 (d, *J* = 8.4 Hz, 1H), 6.30 (d, *J* = 8.7 Hz, 1H), 6.01 (t, *J* = 6.6 Hz, 1H), 5.83 (d, *J* = 8.9 Hz, 1H), 2.43 (s, 8H). **^{31}P{^{1}H} NMR** (202 MHz, DMSO) δ 47.54, -6.00.

CO_2 hydrogenation by 1'. In a glovebox under a nitrogen atmosphere, a J. young NMR tube was charged with complex **1'** (43.5 mg, 0.042 mmol) in 0.5 mL DMSO-d_6. J young NMR tube was taken out from the glovebox, and the NMR tube was purged with an H_2: CO_2 (2:1) mixture to ensure a complete H_2:CO_2 environment in the NMR tube. After that, the NMR tube was closed and placed in a preheated oil bath at 80 °C, then heated overnight. NMR spectroscopy was used to analyze product **3** as the generation of formate peak was observed at δ 8.58 ppm. **^{1}H NMR** (500 MHz, DMSO-d_6, 25°C) δ 10.23 (d, *J* = 5.9 Hz, 1H), 9.70 (d, *J* = 5.7 Hz, 1H), 9.49 (d, *J* = 6.3 Hz, 1H), 8.58 (s, 0.1H), 7.98 (d, *J* = 8.0 Hz, 2H), 7.88 (d, *J* = 8.2 Hz, 1H), 7.85 (s, 1H), 7.64 (d, *J* = 8.2 Hz, 3H), 7.54 (d, *J* = 5.9 Hz, 3H), 7.49 (d, *J* = 7.8 Hz, 3H), 7.44 (d, *J* = 11.6 Hz, 2H), 7.39 (d, *J* = 3.1 Hz, 25H), 7.25 (d, *J* = 3.8 Hz, 13H), 7.20 – 7.14 (m, 5H), 7.05 (t, *J* = 8.0 Hz, 18H), 6.86 (t, *J* = 8.9 Hz, 8H), 6.65 (d, *J* = 8.4 Hz, 2H), 6.48 (d, *J* = 8.8 Hz, 1H), 6.18 (s, 1H), 2.43 (s, 6H). **^{31}P{^{1}H} NMR** (202 MHz, DMSO-d_6, 25°C) δ 51.89, 49.50, -6.00.

CO_2 capture by 1'. In a glovebox under a nitrogen atmosphere, a J young NMR tube was charged with complex **1'** (43.5 mg, 0.042 mmol) in 0.5 mL DMSO-d_6. J Young NMR tube was taken out from the glovebox, and the tube was purged with CO_2 to ensure a complete CO_2 environment in the NMR tube. After that, the NMR tube was closed under the CO_2 environment and placed in a preheated oil bath at 80 °C, then heated overnight. NMR spectroscopy was used to analyze product **4**. **^{1}H NMR** (400 MHz, DMSO-d_6, 25°C) δ 10.24 (d, *J* = 7.8 Hz, 1H), 9.71 (d, *J* = 7.9 Hz, 2H), 7.98 (d, *J* = 8.1 Hz, 5H), 7.92 – 7.82 (m, 7H), 7.76 (d, *J* = 4.6 Hz, 2H), 7.65 – 7.59 (m, 13H), 7.54 (t, *J* = 7.3 Hz, 11H), 7.48 (d, *J* = 8.2 Hz, 7H), 7.44 (d, *J* = 8.1 Hz, 2H), 7.37 (d, *J* = 6.1 Hz, 63H), 7.24 (t, *J* = 6.7 Hz, 34H), 7.11 – 6.98 (m, 6H), 6.95 – 6.82 (m, 8H), 6.65 (d, *J* = 8.2 Hz, 5H), 2.42 (s, 6H). **^{31}P{^{1}H} NMR** (202 MHz, DMSO-d_6, 25°C) δ 48.31, 38.87, 30.65, 25.02, -6.00. **^{13}C{^{1}H} NMR** (126 MHz, DMSO-d_6, 25°C) δ 193.3, 155.5, 154.1, 153.6, 151.9, 148.0, 141.8, 139.9, 139.0, 138.5, 136.1 (d, *J* = 7.4 Hz), 133.3 (d, *J* = 18.8 Hz), 132.0, 131.5 (d, *J* = 9.2 Hz), 130.6, 129.1, 128.74 (d, *J* = 7.4 Hz), 122.2, 120.1, 117.9, 116.4 (d, *J* = 37.2 Hz), 111.7, 110.5 103.0, 20.80, 20.8.

N-methylation of 1'. A 100 mL pressure tube charged with a mixture of complex **1'** (100 mg, 0.096 mmol) and methyl iodide (8.96 µL, 0.144 mmol) in toluene (10 mL) was heated at 110 °C for 24 h. The mixture was cooled to ambient temperature to get a pale-yellow precipitate. The product was collected by filtration, washed with diethyl ether (3X10 mL), and dried under a vacuum to afford the desired product **5**. Yield: 50 mg (48%). **^{1}H NMR** (400 MHz, DMSO-d_6, 25 ºC) δ 9.44 (d, *J* = 4.3 Hz, 1H), 8.13 (d, *J* = 8.3 Hz, 1H), 7.81 – 7.63 (m, 3H), 7.50 (dd, *J* = 32.2, 7.7 Hz, 5H), 7.36 (d, *J* = 8.3 Hz, 2H), 7.30 (t, *J* = 7.0 Hz, 5H), 7.15 (t, *J* = 6.5 Hz, 5H), 7.06 (t, *J* = 8.7 Hz, 9H), 6.81 (t, *J* = 6.7 Hz, 2H), 6.61 (d, *J* = 8.9 Hz, 2H), 6.41 (d, *J* = 8.3 Hz, 2H), 4.52 (s, 3H), 2.46 (s, 3H). **^{13}C {^{1}H} NMR** (100 MHz, DMSO-d_6, 25ºC) δ 205.8 (Ru-CNHC) δ 159.4, 159.0, 158.2, 145.7, 145.1, 144.9, 144.2, 143.5, 142.6, 137.8 (d, *J* = 9.5 Hz), 137.4, 136.4, 136.1, 136.0, 135.4, 135.2, 133.4 (d, *J* = 9.2 Hz), 129.9, 129.5, 122.8, 122.3, 119.0, 117.2, 116.4, 110.6, 39.7, 26.1.**^{31}P{^{1}H} NMR** (162 MHz, DMSO-d_6,25ºC) δ = 31.48 ppm. HRMS (ESI^+) m/z calcd for $C_{61}H_{51}ClN_5P_2Ru$, $[M\text{-}I]^+$, 1052.2359, found 1052.2381.

Terminal alkyne activation by 1'. In a J. Young NMR tube, complex **1'** (50 mg, 0.048 mmol) was dissolved in DMSO-d_6 (0.5 mL). Then, phenylacetylene (0.072 mmol, 7.90 µL) was added to the homogeneous solution. The resulting mixture was placed in a preheated oil bath at 80 °C for 12 h. The ^{1}H NMR analysis shows singlets at δ 13.52 and 13.92 ppm for the NH functionality of **6** and **6a**, respectively. ^{31}P{^{1}H} NMR analysis shows the signals at δ 32.43 and 49.00 ppm for **6** and **6a**, respectively. **^{1}H NMR** (500 MHz, DMSO-d_6, 25°C) δ 13.52 (s, 1H), 10.24 (d, *J* = 6.0 Hz, 2H), 9.71 (d, *J* = 5.6 Hz, 2H), 9.52 (d, *J* = 6.1 Hz, 1H), 9.47 (d, *J* = 6.3 Hz, 2H), 9.10 (dd, *J* = 12.1, 6.0 Hz, 3H), 8.93 (s, 0H), 8.37 (d, *J* = 4.8 Hz, 0H), 7.99 (t, *J* = 7.4 Hz, 2H), 7.94 (d, *J* = 7.9 Hz, 2H), 7.89 (t, *J* = 8.2 Hz, 1H), 7.84 (d, *J* = 8.0 Hz, 2H), 7.78 (q, *J* = 7.2 Hz, 4H), 7.66 – 7.61 (m, 5H), 7.55 – 7.50 (m, 6H), 7.50 – 7.44 (m, 7H), 7.38 (d, *J* = 3.8 Hz, 37H), 7.24 (dt, *J* = 6.9, 3.2 Hz, 26H), 7.18 (d, *J* = 10.1 Hz, 12H), 7.04 (s, 20H), 6.92 – 6.83

(m, 14H), 6.65 (d, *J* = 8.2 Hz, 2H), 6.47 (s, 1H), 6.19 (d, *J* = 8.5 Hz, 3H), 2.46 (s, 3H), 2.39 (s, 3H). **^{31}P NMR** (202 MHz, DMSO-d_6, 25°C) δ 49.00, 32.43, -6.00.

X-ray Diffraction Studies

Single crystals of complexes **1**, **2**, and **2',** suitable for X-ray crystallographic determination, were obtained by layering the corresponding complexes in MeOH with Ether (1/3, v/v) at -18 °C. Single crystal X-ray diffraction studies for complexes **1**, **2**, and **2'** were carried out using dual-core Agilent technology (Oxford diffraction) super Nova CCD system, with monochromated Mo−Kα radiation (λ = 0.71073 Å). Unit cell determination, data collection and reduction, and empirical absorption correction were performed using the CrysAlisPro program. The Olex 2-1.5 program[30] was used as the graphical interface. The structures were solved by direct methods using SHELXT,[31] which revealed the positions of all not-disordered non-hydrogen atoms. The structure model was refined using full matrix least squares minimization on F^2 using ShelXL[32] within Olex2 for a graphical interface. The non-hydrogen atoms were refined anisotropically. All hydrogen positions were fixed in place for the final refinement cycles. Deposition Number(s) <url href="https://www.ccdc.cam.ac.uk/services/structures?id=doi:10.1002/chem.202301971"> 2238659 (for **1**), 2238661 (for **2**), 2238660 (for **2'**)</url> contain the supplementary crystallographic data for this paper. These data are provided free of charge by the joint Cambridge Crystallographic Data Centre and Fachinformationszentrum Karlsruhe <url href="http://www.ccdc.cam.ac.uk/structures">Access Structures service</url>.

Computational details

All DFT calculations were performed using the ORCA 5.0.3 program package developed by Neese and co-workers.[33]The geometry optimizations were carried out using r^2scan-3c composite functional, which has been shown to produce excellent geometries for transition metal complexes.[34] The r^2scan-3c uses a modified triple-ζ basis, def2-mTZVPP (BS1), along with auxiliary basis def2-mTZVPP/J for Resolution of Identity (RI) approximation and def2-ECP on heavier elements (Ru and I), Grimme's atom-pairwise dispersion correction (D4), and a geometric counterpoise correction (gCP). Single point calculations were performed on the optimized geometries using M06 hybrid functional with def2-QZVP and def2-ECP on Ruthenium and def2-TZVP(-f) (BS2) on all other atoms. Grimme's dispersion correction (D3Zero) and ORCA's inbuilt finer integration grid "DEFGRID3" was used during the final single point calculation. Tight SCF convergence criterion and a solvent model in which methanol is described by an implicit conductor-like polarizable continuum medium (CPCM) were used during all calculations. The results of single-point calculations at M06/BS2 level were used to perform NPA analysis using JANPA software.[35]

Acknowledgements

AKS acknowledges SERB, India, for financial support in the form of the project (EMR/2016/004076). SN acknowledges CSIR New Delhi, and EY acknowledges IIT Indore for fellowship. AR is thankful to SERB, India for NPDF fellowship (PDF/2016/001786) All authors gratefully acknowledge SIC, IIT Indore, and DST-First 500 MHz NMR facility, Department of chemistry IIT Indore, for sample characterization.

Keywords: Metal-ligand cooperativity • Anionic-naked-NHC • Small molecule activation • H_2 splitting • CO_2 capture

[1] a) S. Kuwata, F. E. Hahn, *Chem. Rev.* **2018**, *118*, 9642–9677; b) M. C. Jahnke, F. E. Hahn, *Coord. Chem. Rev.* **2015**, *293–294*, 95–115; c) T. Toda, A. Yoshinari, T. Ikariya, S. Kuwata, *Chem. Eur. J.* **2016**, *22*, 16675–16683; d) W. Chang, X. Gong, S. Wang, L.-P. Xiao, G. Song, *Org. Biomol. Chem.* **2017**, *15*, 3466–3471; e) S. Kuwata, T. Ikariya, *ChemComm.* **2014**, *50*, 14290–14300; f) B. T. H. Tsui, M. M. H. Sung, J. Kinas, F. E. Hahn, R. H. Morris, *Organometallics* **2022**, *41*, 2095–2105.

[2] a) D. C. Marelius, E. H. Darrow, C. E. Moore, J. A. Golen, A. L. Rheingold, D. B. Grotjahn, *Chem. Eur. J.* **2015**, *21*, 10988–10992; b) J. L. Gomez-Lopez, D. Chávez, M. Parra-Hake, A. T. Royappa, A. L. Rheingold, D. B. Grotjahn, V. Miranda-Soto, *Organometallics* **2016**, *35*, 3148–3153; c) M. K. Rong, A. Chirila, D. Franciolus, M. Lutz, M. Nieger, A. W. Ehlers, J. C. Slootweg, K. Lammertsma, *Organometallics* **2019**, *38*, 4543–4553; d) M. C. Jahnke, F. E. Hahn, *Chem. Lett.* **2015**, *44*, 226–237; e) C. Mühlen, J. Linde, L. Rakers, T. T. Y. Tan, F. Kampert, F. Glorius, F. E. Hahn, *Organometallics* **2019**, *38*, 2417–2421; f) S. Cepa, C. Schulte to Brinke, F. Roelfes, F. E. Hahn, *Organometallics* **2015**, *34*, 5454–5460; g) D. B. Grotjahn, J. K. Martin, T. N. Tom, A. L. Rheingold, *Inorganics* **2018**, *6*, 27; h) F. He, P. Braunstein, M. Wesolek, A. A. Danopoulos, *ChemComm.* **2015**, *51*, 2814–2817.

[3] a) T. Kösterke, J. Kösters, E.-U. Würthwein, C. Mück-Lichtenfeld, C. Schulte to Brinke, F. Lahoz, F. E. Hahn, *Chem. Eur. J.* **2012**, *18*, 14594–14598; b) V. César, N. Lugan, G. Lavigne, *J. Am. Chem. Soc.* **2008**, *130*, 11286–11287; c) F. E. Hahn, *ChemCatChem* **2013**, *5*, 419–430; d) S. T. Liddle, I. S. Edworthy, P. L. Arnold, *Chem. Soc. Rev.* **2007**, *36*, 1732; e) M. Leow, C. Ho, M. Gardiner, A. Bissember, *Catalysts* **2018**, *8*, 620.

[4] a) T. Toda, S. Kuwata, T. Ikariya, *Chem. Eur. J.* **2014**, *20*, 9539–9542; b) W. Chang, X. Gong, S. Wang, L.-P. Xiao, G. Song, *Org. Biomol. Chem.* **2017**, *15*, 3466–3471.

[5] a) M. Poyatos, J. A. Mata, E. Peris, *Chem. Rev.* **2009**, *109*, 3677–3707; b) S. Díez-González, N. Marion, S. P. Nolan, *Chem. Rev.* **2009**, *109*, 3612–3676; c) E. Peris, *Chem. Rev.* **2018**, *118*, 9988–10031; d) V. M. Chernyshev, E. A. Denisova, D. B. Eremin, V. P. Ananikov, *Chem. Sci.* **2020**, *11*, 6957–6977.

[6] a) H. Li, B. Zheng, K.-W. Huang, *Coord Chem Rev* **2015**, *293–294*, 116–138; b) T. Higashi, S. Kusumoto, K. Nozaki, *Chem. Rev.* **2019**, *119*, 10393–10402; c) J. R. Khusnutdinova, D. Milstein, *Angew. Chem. Int. Ed.* **2015**, *54*, 12236–12273; d) C. Gunanathan, D. Milstein, *Acc. Chem. Res.* **2011**, *44*, 588–602; e) M. R. Elsby, R. T. Baker, *Chem. Soc. Rev.* **2020**, *49*, 8933–8987 f) T. P. Gonçalves, I. Dutta, K.-W. Huang, *ChemComm* **2021**, *57*, 3070–3082; g) M. D. Wodrich, X. Hu, *Nat Rev Chem* **2017**, *2*, 0099.

[7] a) J. J. Kiernicki, M. Zeller, N. K. Szymczak, *Inorg. Chem.* **2020**, *59*, 9279–9286; b)S. Kuwata, T. Ikariya, *Chem. Eur. J.* **2011**, *17*, 3542–3556; c) L.-P. He, T. Chen, D. Gong, Z. Lai, K.-W. Huang, *Organometallics* **2012**, *31*, 5208–5211; d) M. Kaur, N. U Din Reshi, K. Patra, A. Bhattacherya, S. Kunnikuruvan, J. K. Bera, *Chem. Eur. J.* **2021**, *27*, 10737–10748; e) J. B. Geri, N. K. Szymczak, *J. Am. Chem. Soc.* **2015**, *137*, 12808–12814; f) J. Shi, B. Hu, D. Gong, S. Shang, G. Hou, D. Chen, *Dalton Trans.* **2016**, *45*, 4828–4834; g) H. Li, T. P. Gonçalves, D. Lupp, K.-W. Huang, *ACS Catal.* **2019**, *9*, 1619–1629.

[8] R. Noyori, *Asymmetric Catalysis* **2002**, 15.

[9] a) P. G. Jessop, T. Ikariya, R. Noyori, *Nature* **1994**, *368*, 231-233**;** b) R. Noyori, T. Ohkuma, *Angew. Chem. Int. Ed.* **2001**, *40*, 40–73; c) T. Ikariya, K. Murata, R. Noyori, *Org. Biomol. Chem.* **2006**, *4*, 393–406; d)

K.-J. Haack, S. Hashiguchi, A. Fujii, T. Ikariya, R. Noyori, *Angew. Chem. Int. Ed. Engl.* **1997**, *36*, 285–288; e) M. Yamakawa, H. Ito, R. Noyori, *J. Am. Chem. Soc.* **2000**, *122*, 1466–1478; f) A. Fujii, S. Hashiguchi, N. Uematsu, T. Ikariya, R. Noyori, *J. Am. Chem. Soc.* **1996**, *118*, 2521–2522; g)C. A. Sandoval, T. Ohkuma, K. Muñiz, R. Noyori, *J. Am. Chem. Soc.* **2003**, *125*, 13490–13503.

[10] M. C. Johnson, D. Rogers, W. Kaminsky, B. M. Cossairt, *Inorg. Chem.* **2021**, *60*, 5996–6003.

[11] a) F. He, M. Wesolek, A. A. Danopoulos, P. Braunstein, *Chem. Eur. J.* **2016**, *22*, 2658–2671; b) R. Das, A. Hepp, C. G. Daniliuc, F. E. Hahn, *Organometallics* **2014**, *33*, 6975–6987.

[12] a)D. W. Stephan, *J. Am. Chem. Soc.* **2015**, *137*, 10018–10032; b) D. W. Stephan, *Acc. Chem. Res.* **2015**, *48*, 306–316; c) G. Erker, D. W. Stephan, Eds. , *Frustrated Lewis Pairs I: Uncovering and Understanding*, Springer Berlin Heidelberg, Berlin, Heidelberg, **2013**; d) D. J. Scott, T. R. Simmons, E. J. Lawrence, G. G. Wildgoose, M. J. Fuchter, A. E. Ashley, *ACS Catal.* **2015**, *5*, 5540–5544; e) D. J. Scott, M. J. Fuchter, A. E. Ashley, *Angew. Chem.* **2014**, *126*, 10382–10386; f) G. Erker, , *C R Chim* **2011**, *14*, 831–841; g) Á. Gyömöre, M. Bakos, T. Földes, I. Pápai, A. Domján, T. Soós, *ACS Catal.* **2015**, *5*, 5366–5372; h) D. W. Stephan, *Org. Biomol. Chem.* **2012**, *10*, 5740; i) D. W. Stephan, *Org. Biomol. Chem.* **2008**, *6*, 1535; j) M. Sajid, A. Klose, B. Birkmann, L. Liang, B. Schirmer, T. Wiegand, H. Eckert, A. J. Lough, R. Fröhlich, C. G. Daniliuc, S. Grimme, D. W. Stephan, G. Kehr, G. Erker, *Chem. Sci.* **2013**, *4*, 213–219; k) P. Spies, G. Erker, G. Kehr, K. Bergander, R. Fröhlich, S. Grimme, D. W. Stephan, *ChemComm.* **2007**, 5072.

[13] E. R. M. Habraken, A. R. Jupp, M. B. Brands, M. Nieger, A. W. Ehlers, J. C. Slootweg, *Eur. J. Inorg. Chem.* **2019**, *2019*, 2436–2442.

[14] a) R. Pal, M. Ghara, P. K. Chattaraj, *Catalysts* **2022**, *12*, 201; b) J. Zeng, R. Qiu, J. Zhu, *Chem Asian J* **2023**, *18*, DOI 10.1002/asia.202201236; c) M. T. Whited, *Beilstein J. Org. Chem.* **2012**, *8*, 1554–1563; d) S. Das, R. Laplaza, J. T. Blaskovits, C. Corminboeuf, *Angew. Chem. Int. Ed.* **2022**, *61*, e202202727; e) N. von Wolff, G. Lefèvre, J.-C. Berthet, P. Thuéry, T. Cantat, *ACS Catal.* **2016**, *6*, 4526–4535; f) X. Xu, G. Kehr, C. G. Daniliuc, G. Erker, *J. Am. Chem. Soc.* **2013**, *135*, 6465–6476; g) Z. Mo, E. L. Kolychev, A. Rit, J. Campos, H. Niu, S. Aldridge, *J. Am. Chem. Soc.* **2015**, *137*, 12227–12230; h) C. M. Mömming, S. Frömel, G. Kehr, R. Fröhlich, S. Grimme, G. Erker, *J. Am. Chem. Soc.* **2009**, *131*, 12280–12289.

[15] a) A. M. Chapman, M. F. Haddow, D. F. Wass, *J. Am. Chem. Soc.* **2011**, *133*, 18463–18478; b) A. Coffinet, D. Specklin, L. Vendier, M. Etienne, A. Simonneau, *Chem. Eur. J.* **2019**, *25*, 14300–14303; c) A. Simonneau, R. Turrel, L. Vendier, M. Etienne, *Angew. Chem.* **2017**, *129*, 12436–12440; d) S. R. Flynn, D. F. Wass, *ACS Catal.* **2013**, *3*, 2574–2581; e) S. Geier, Transition Metal Complexes and Main Group Frustrated Lewis Pairs for Stoichiometric and Catalytic P-P and H-H Bond Activation, Thesis, University of Toronto (Canada), **2011**; f) A. M. Chapman, S. R. Flynn, D. F. Wass, *Inorg. Chem.* **2016**, *55*, 1017–1021; g) S. Burling, M. F. Mahon, R. E. Powell, M. K. Whittlesey, J. M. J. Williams, *J. Am. Chem. Soc.* **2006**, *128*, 13702–13703; h) C. Ferrer, J. Ferrer, V. Passarelli, F. J. Lahoz, P. García-Orduña, D. Carmona, *Organometallics* **2022**, *41*, 1445–1453.

[16] a) Q. J. Bruch, A. Tanushi, P. Müller, A. T. Radosevich, *J. Am. Chem. Soc.* **2022**, *144*, 21443–21447; b) D. W. Stephan, G. Erker, *Chem. Sci.* **2014**, *5*, 2625–2641; c) K. Chernichenko, Á. Madarász, I. Pápai, M. Nieger, M. Leskelä, T. Repo, *Nat Chem* **2013**, *5*, 718–723.

[17] F. Bertini, V. Lyaskovskyy, B. J. J. Timmer, F. J. J. de Kanter, M. Lutz, A. W. Ehlers, J. C. Slootweg, K. Lammertsma, *J. Am. Chem. Soc.* **2012**, *134*, 201–204.

[18] a) M. Navarro, J. J. Moreno, *ChemComm.* **2022**, *58*, 11220–11235; b) S. R. Flynn, O. J. Metters, I. Manners, D. F. Wass, *Organometallics* **2016**, *35*, 847–850; c) M. A. Stevens, A. L. Colebatch, *Chem. Soc. Rev.* **2022**, *51*, 1881–1898; d) K. Mistry, P. G. Pringle, H. A. Sparkes, D. F. Wass, *Organometallics* **2020**, *39*, 468–477.

[19] a) L. Wang, N. Liu, B. Dai, H. Hu, *Eur. J. Org. Chem.* **2014**, *2014*, 6493–6500; b) M. M. Heravi, Z. Kheilkordi, V. Zadsirjan, M. Heydari, M. Malmir, *J. Organomet Chem* **2018**, *861*, 17–104.

[20] C. F. Harris, D. A. K. Vezzu, L. Bartolotti, P. D. Boyle, S. Huo, *Inorg. Chem.* **2013**, *52*, 11711–11722.

[21] a) V. Miranda-Soto, D. B. Grotjahn, A. L. Cooksy, J. A. Golen, C. E. Moore, A. L. Rheingold, *Angew. Chem. Int. Ed.* **2011**, *50*, 631–635; b) S. E. Flowers, B. M. Cossairt, *Organometallics* **2014**, *33*, 4341–4344; c) K. Araki, S. Kuwata, T. Ikariya, *Organometallics* **2008**, *27*, 2176–2178.

[22] M. G. Tay, T. Lokanathan, K. T. Ong, R. A. Abu Talip, Y. Y. Chia, *Int. J. Inorg* **2016**, *2016*, 1–5.

[23] K. Voigtritter, S. Ghorai, B. H. Lipshutz, *J. Org. Chem.* **2011**, *76*, 4697–4702.

[24] a) T. Ohkuma, M. Koizumi, K. Muñiz, G. Hilt, C. Kabuto, R. Noyori, *J. Am. Chem. Soc.* **2002**, *124*, 6508–6509; b) M. K. Cybulski, N. A. Beattie, S. A. Macgregor, M. F. Mahon, M. K. Whittlesey, *Chem. Eur. J.* **2020**, *26*, 11141–11145.

[25] a) R. Das, C. G. Daniliuc, F. E. Hahn, *Angew. Chem. Int. Ed.* **2014**, *53*, 1163–1166; b) M. C. Jahnke, A. Herve, F. Kampert, F. E. Hahn, *Inorg. Chim. Acta* **2021**, *515*, 120055; c) A. A. Danopoulos, K. Yu. Monakhov, P. Braunstein, *Chem. Eur. J.* **2013**, *19*, 450–455; d) E. E. Martinez, C. A. Jensen, A. J. S. Larson, K. C. Kenney, K. J. Clark, S. H. Nazari, G. A. Valdivia-Berroeta, S. J. Smith, D. H. Ess, D. J. Michaelis, *Adv. Synth. Catal.* **2020**, *362*, 2876–2881.

[26] a) M. A. Dureen, D. W. Stephan, *J. Am. Chem. Soc.* **2009**, *131*, 8396–8397; b) C. Jiang, O. Blacque, H. Berke, *Organometallics* **2010**, *29*, 125–133.

[27] B. Maji, A. Kumar, A. Bhattacherya, J. K. Bera, J. Choudhury, *Organometallics* **2022**, *41*, 3589–3599.

[28] a) T. Gasevic, J. B. Stückrath, S. Grimme, M. Bursch, *J. Phys. Chem. A* **2022**, *126*, 3826–3838 ; b) S. Grimme, A. Hansen, S. Ehlert, J.-M. Mewes, *J. Chem. Phys.* **2021**, *154*, 064103.

[29] H. I. Schlesinger, M. W. Tapley, D. H. Brown, R. D. Peacock, W. L. Jolly, T. C. Waddington, *J. Am. Chem. Soc.* **1924,** *46***,** 276

[30] O. V. Dolomanov, L. J. Bourhis, R. J. Gildea, J. A. K. Howard, H. Puschmann, *J. Appl. Cryst.* **2009**, *42*, 339–341.

[31] G. M. Sheldrick, *Acta Cryst.* **2015**, *71*, 3–8.

[32] G. M. Sheldrick, *Acta Cryst.* **2008**, *64*, 112–122.

[33] a) F. Neese, *WIREs Comput Mol Sci* **2012**, *2*, 73–78; b) F. Neese, F. Wennmohs, U. Becker, C. Riplinger, *J. Chem. Phys.* **2020**, *152*, 224108; c) F. Neese, *WIREs Comput Mol Sci* **2022**, *12*, DOI 10.1002/wcms.1606.

[34] J. G. Brandenburg, C. Bannwarth, A. Hansen, S. Grimme, *J. Phys. chem. A* **2018**, *148*, 064104.

[35] T. Y. Nikolaienko, L. A. Bulavin, D. M. Hovorun, *Comput. Theor. Chem.* **2014**, *1050*, 15–22.